

1     **A GENERALISED RANDOM ENCOUNTER MODEL FOR ESTIMATING**  
2                     **ANIMAL DENSITY WITH REMOTE SENSOR DATA**

3     **Running title: A generalised random encounter model for animals.**

4     **Word count:**

5     **Authors:**

6     Tim C.D. Lucas<sup>1,2,3</sup>, Elizabeth A. Moorcroft<sup>1,4,5</sup>, Robin Freeman<sup>5</sup>, Marcus J. Rowcliffe<sup>5</sup>,  
7     Kate E. Jones<sup>2,5</sup>

8     **Addresses:**

9     1 CoMPLEX, University College London, Physics Building, Gower Street, Lon-  
10     don, WC1E 6BT, UK

11    2 Centre for Biodiversity and Environment Research, Department of Genetics,  
12     Evolution and Environment, University College London, Gower Street, London,  
13     WC1E 6BT, UK

14    3 Department of Statistical Science, University College London, Gower Street,  
15     London, WC1E 6BT, UK

16    4 Department of Computer Science, University College London, Gower Street,  
17     London, WC1E 6BT, UK

18    5 Institute of Zoology, Zoological Society of London, Regents Park, London, NW1  
19     4RY, UK

20    **Corresponding authors:**

21    Kate E. Jones,  
22    Centre for Biodiversity and Environment Research,  
23    Department of Genetics, Evolution and Environment,  
24    University College London,  
25    Gower Street,  
26    London,  
27    WC1E 6BT,  
28    UK

29 kate.e.jones@ucl.ac.uk

30

31 Marcus J. Rowcliffe,

32 Institute of Zoology,

33 Zoological Society of London,

34 Regents Park,

35 London,

36 NW1 4RY,

37 UK

38 marcus.rowcliffe@ioz.ac.uk

## 1. ABSTRACT

**1:** Wildlife monitoring technology has advanced rapidly and the use of remote sensors such as camera traps, and acoustic detectors is becoming common in both the terrestrial and marine environments. Current capture-recapture or distance methods to estimate abundance or density require individual recognition of animals or knowing the distance of the animal from the sensor, which is often difficult. A method without these requirements, the random encounter model (REM), has been successfully applied to estimate animal densities from count data generated from camera traps. However, count data from acoustic detectors do not fit the assumptions of the REM due to the directionality of animal signals.

**2:** We developed a generalised REM (gREM), to estimate absolute animal density from count data from both camera traps and acoustic detectors. We derived the gREM for different combinations of sensor detection widths and animal signal widths (a measure of directionality). We tested the accuracy and precision of this model using simulations of different combinations of sensor detection widths and animal signal widths, number of captures, and models of animal movement.

**3:** We find that the gREM produces accurate estimates of absolute animal density for all combinations of sensor detection widths and animal signal widths. However, larger sensor detection and animal signal widths were found to be more precise. While the model is accurate for all capture efforts tested, the precision of the estimate increases with the number of captures. We found no effect of different animal movement models tested on the accuracy and precision of the gREM.

**4:** We conclude that the gREM provides an effective method to estimate absolute animal densities from remote sensor count data over a range of sensor and animal signal widths. The gREM is applicable for use for count data obtained in both marine and terrestrial environments, visually or acoustically (e.g., big cats, sharks, birds, bats and cetaceans). As sensors such as camera traps and acoustic detectors become more ubiquitous, the gREM will be increasingly useful for monitoring animal populations across broad spatial, temporal and taxonomic scales.

68 1.1. **Keywords.** Acoustic detection, Camera traps, Marine, Population monitor-  
69 ing, Simulations, Terrestrial

## 70 2. INTRODUCTION

71 Animal population density is one of the fundamental measures needed in ecol-  
72 ogy and conservation. The density of a population has important implications  
73 for a range of issues such as sensitivity to stochastic fluctuations (??) and risk  
74 of extinction (?). Monitoring animal population changes in response to anthro-  
75 pogenic pressure is becoming increasingly important as humans modify habi-  
76 tats and change climates as never before (?). Sensor technology, such as camera  
77 traps (??) and acoustic detectors (???) are becoming increasingly used to monitor  
78 changes in animal populations (??), as they are efficient, relatively cheap and non-  
79 invasive (?), allowing for surveys over large areas and long periods. However,  
80 the problem of converting sampled count data to estimates of density remains as  
81 efforts must be made to account for detectability of the animals (?).

82 Methods do already exist for estimating animal density if the distance between  
83 the animal and the sensor can be estimated (e.g., capture-mark recapture methods  
84 (?) and distance sampling (?)). However, these methods often require additional  
85 information that may not be available. For example, capture-mark-recapture meth-  
86 ods (????) require recognition of individuals; distance methods require a distance  
87 estimation of how far away individuals are from the sensor barlow2005estimates,  
88 marques2011estimating. The development of the random encounter model (REM)  
89 (a modification of a gas model) enabled animal densities to be estimated from un-  
90 marked individuals of a known speed, and sensor detection parameters (?). The  
91 REM method has been successfully applied to estimate animal densities from cam-  
92 era trap surveys (??). However, extending the REM method to other types of  
93 sensors (for example acoustic detectors) is more problematic, because the origi-  
94 nal derivation assumes a relatively narrow sensor width (up to  $\pi/2$  radians) and  
95 that the animal is equally detectable irrespective of its heading (?).

96 Whilst these restrictions are not problematic for most camera trap makes (e.g.  
97 Reconyx, Cuddeback), the REM could not be used to estimate densities from cam-  
98 era traps with a wider sensor width (e.g. canopy monitoring with fish eye lens

(?). Additionally, the REM method would not be useful in estimating densities from acoustic survey data as the acoustic detector angles are often wider than  $\pi/2$  radians. Acoustic detectors are designed for a range of diverse tasks and environments (?), which will naturally lead to a wide range of sensor detection widths and detection distances. In addition to this, calls emitted by many animals are directional (breaking the assumption of the REM method).

There has been a sharp rise in interest around passive acoustic detectors in recent years, with a 10 fold increase in publications in the decade between 2000 and 2010 (?). Acoustic monitoring is being developed to study many aspects of ecology, including the interactions of animals and their environments (??), the presence and relative abundances of species (?), and biodiversity of an area (?).

Acoustic data suffers from many of the problems associated with data from camera trap surveys in that individuals are often unmarked so capture-make-recapture methods cannot be used to estimate densities. In some cases the distance between the animal and the sensor is known, for example when an array of sensors and the position of the animal is estimated by triangulation (?). In these situations distance-sampling methods can be applied, a method typically used for marine mammals (?). However, in many cases distance estimation is not possible, for example when single sensors are deployed, a situation typical in the majority of terrestrial acoustic surveys (??). In these cases, only relative measures of local abundance can be calculated, and not absolute densities. This means that comparison of populations between species and sites is problematic without assuming equal detectability (?). Equality detectability is unlikely because of differences in environmental conditions, sensor type, habitats, species biology.

In this study we create a generalised REM (gREM), as an extension to the camera trap model of (?), to estimate absolute density from count data from acoustic detectors, or camera traps, where the sensor width can vary from 0 to  $2\pi$  radians, and the signal given off from the animal can be directional. We assessed the accuracy and precision of the gREM within a simulated environment, by varying the sensor detection widths, animal signal widths, number of captures and models of animal movement. We use the simulation results to recommend best survey practice for estimating animal densities from remote sensors.

### 3. METHODS

131  
132 **3.1. Analytical Model.** The REM presented by (?) adapts the gas model to model  
133 count data from camera trap surveys. The REM is derived assuming a stationary  
134 sensor with a detection width less than  $\pi/2$  radians. However, in order to apply  
135 this approach more generally, and in particular to acoustic detectors, we need both  
136 to relax the constraint on sensor detection width, and allow for animals with di-  
137 rectional signals. Consequently, we derive the gREM for any detection width,  $\theta$ ,  
138 between 0 and  $2\pi$  with a detection distance  $r$  giving a circular sector within which  
139 animals can be captured (the detection zone)(Figure 1). Additionally, we model  
140 the animal as having an associated signal width  $\alpha$  between 0 and  $2\pi$ (Figure 1, see  
141 Appendix S1 for a list of symbols). We start deriving the gREM with the simplest  
142 situation, the gas model where  $\theta = 2\pi$  and  $\alpha = 2\pi$ .

143 **3.1.1. Gas Model.** Following ?, we derive the gas model where sensors can capture  
144 animals in any direction and animal's signal is detectable from any direction( $\theta =$   
145  $2\pi$  and  $\alpha = 2\pi$ ). We assume that animals are in a homogeneous environment,  
146 and move in straight lines of random direction with velocity  $v$ . We allow that  
147 our stationary sensor can capture animals at a detection distance  $r$  and that if an  
148 animal moves within this detection zone they are captured with a probability of  
149 one, while animals outside the zone are never captured.

150 In order to derive animal density, we need to consider relative velocity from  
151 the reference frame of the animals. Conceptually, this requires us to imagine that  
152 all animals are stationary and randomly distributed in space, while the sensor  
153 moves with velocity  $v$ . If we calculate the area covered by the sensor during the  
154 survey period we can estimate the number of animals the sensor should capture.  
155 As a circle moving across a plane, the area covered by the sensor per unit time is  
156  $2rv$ . The number of expected captures,  $z$ , for a survey period of  $t$ , with an animal  
157 density of  $D$  is  $z = 2rvtD$ . To estimate the density, we rearrange to get  $D = z/2rvt$ .

158 **3.1.2. gREM derivations for different detection and signal widths.** Different combina-  
159 tions of  $\theta$  and  $\alpha$  would be expected to occur (e.g., sensors have different detection  
160 widths and animals have different signal widths). For different combinations  $\theta$   
161 and  $\alpha$ , the area covered per unit time is no longer given by  $2rv$ . Instead of the size

162 of the sensor detection zone having a diameter of  $2r$ , the size changes with the  
 163 approach angle between the sensor and the animal. For any given signal width  
 164 and detector width and depending on the angle that the animal approaches the  
 165 sensor, the width of the area within which an animal can be detected is called the  
 166 profile,  $p$ . The size of the profile (averaged across all approach angles) is defined  
 167 as the average profile  $\bar{p}$ . However, different combinations of  $\theta$  and  $\alpha$  need different  
 168 equations to calculate  $\bar{p}$ .

169 We have identified the parameter space for the combinations of  $\theta$  and  $\alpha$  for  
 170 which the derivation of the equations are the same (defined as sub-models in the  
 171 gREM) (Figure 2). For example, the gas model becomes the simplest gREM sub-  
 172 model (upper right in (Figure 2) and the REM from (?) is another gREM sub-model  
 173 where  $\theta < \pi/2$  and  $\alpha = 2\pi$ . We derive one gREM sub-model SE2 as an example  
 174 below (where  $4\pi - 2\alpha < \theta < 2\pi$ ,  $0 < \alpha < \pi$ ) (see Appendix S2 for other gREM  
 175 sub-models).

176 3.1.3. *Example derivation of SE2.* In order to calculate  $\bar{p}$ , we have to integrate over  
 177 the focal angle,  $x_1$  (Figure 3a). This is the angle taken from the centre line of the  
 178 sensor. Other focal angles are possible ( $x_2, x_3, x_4$ ) and are used in other gREM  
 179 sub-models (see Appendix S2). As the size of the profile depends on the approach  
 180 angle, we present the derivation across all approach angles. When the sensor is  
 181 directly approaching the animal  $x_1 = \pi/2$ .

182 Starting from  $x_1 = \pi/2$  until  $\theta/2 + \pi/2 - \alpha/2$ , the size of the profile is  $2r \sin \alpha/2$   
 183 (Figure 3b). During this first interval, the size of  $\alpha$  limits the width of the profile.  
 184 When the animal reaches  $x_1 = \theta/2 + \pi/2 - \alpha/2$  (Figure 3c), the size of the profile is  
 185  $r \sin(\alpha/2) + r \cos(x_1 - \theta/2)$  and the size of  $\theta$  and  $\alpha$  both limit the width of the profile  
 186 (Figure 3c). Finally, at  $x_1 = 5\pi/2 - \theta/2 - \alpha/2$  until  $x_1 = 3\pi/2$ , the width of the profile  
 187 is again  $2r \sin \alpha/2$  (Figure 3d) and the size of  $\alpha$  again limits the width of the profile.

188 The profile width  $p$  for  $\pi$  radians of rotation (from directly towards the sensor  
 189 to directly behind the sensor) is completely characterised by the three intervals  
 190 (Figure 3b–3d). Average profile width  $\bar{p}$  is calculated by integrating these profiles  
 191 over their appropriate intervals of  $x_1$  and dividing by  $\pi$  which gives

$$\bar{p} = \frac{1}{\pi} \left( \int_{\frac{\pi}{2}}^{\frac{\pi}{2} + \frac{\theta}{2} - \frac{\alpha}{2}} 2r \sin \frac{\alpha}{2} dx_1 + \int_{\frac{\pi}{2} + \frac{\theta}{2} - \frac{\alpha}{2}}^{\frac{5\pi}{2} - \frac{\theta}{2} - \frac{\alpha}{2}} r \sin \frac{\alpha}{2} + r \cos \left( x_1 - \frac{\theta}{2} \right) dx_1 + \int_{\frac{5\pi}{2} - \frac{\theta}{2} - \frac{\alpha}{2}}^{\frac{3\pi}{2}} 2r \sin \frac{\alpha}{2} dx_1 \right) \quad \text{eqn 1}$$

$$= \frac{r}{\pi} \left( \theta \sin \frac{\alpha}{2} - \cos \frac{\alpha}{2} + \cos \left( \frac{\alpha}{2} + \theta \right) \right) \quad \text{eqn 2}$$

192 We then, as with the gas model, use this expression to calculate density

$$193 \quad D = z/vt\bar{p}. \quad \text{eqn 3}$$

194 Rather than having one equation that describes  $\bar{p}$  globally, the gREM must be  
 195 split into submodels due to discontinuous changes in  $p$  as  $\alpha$  and  $\beta$  change. These  
 196 discontinuities can occur for a number of reasons such as a profile switching be-  
 197 tween being limited by  $\alpha$  and  $\theta$ , the difference between very small profiles and  
 198 profiles of size zero and the fact that the width of a sector stops increasing once  
 199 the central angle reaches  $\pi$  radians (i.e., a semi circle is just as wide as a full circle.)

200 As a visual example, if  $\alpha$  is small, there is an interval between Fig. 3c and 3d  
 201 where the ‘blind spot’ would prevent animals being detected at all giving  $p = 0$ .  
 202 This would require an extra integral in our equation as simply putting our small  
 203 value of  $\alpha$  into eqn 1 would not give us this integral of  $p = 0$ .

204 gREM submodel specifications were done by hand, and the integration was  
 205 done using SymPy (?) in Python (Appendix S3). The gREM submodels were  
 206 checked by confirming that: 1) submodels adjacent in parameter space were equal  
 207 at the boundary between them; 2) submodels that border  $\alpha = 0$  had  $p = 0$  when  
 208  $\alpha = 0$ ; 3) average profile widths  $\bar{p}$  were between 0 and  $2r$  and; 4) each integral, di-  
 209 vided by the range of angles that it was integrated over, was between 0 and  $2r$ . The  
 210 scripts for these tests are included in Appendix S3 and the R (?) implementation  
 211 of the gREM is given in Appendix S4.

212 **3.2. Simulation Model.** We tested the accuracy and precision of the gREM by de-  
 213 veloping a spatially explicit simulation of the interaction of sensors and animals  
 214 using different combinations of sensor detection widths, animal signal widths,  
 215 number of captures, and models of animal movement. 100 simulations were run



where each consisted of a 7.5 km by 7.5 km square (with periodic boundaries). A stationary sensor of radius  $r$  was set up in the exact centre of each simulation, covering 7 sensor detection widths  $\theta$  between 0 and  $2\pi$  ( $2/9\pi, 4/9\pi, 6/9\pi, 8/9\pi, 10/9\pi, 14/9\pi, 2\pi$ ). Each simulation was populated with a density of 70 animals  $\text{km}^{-2}$ , calculated from the equation in ? as the expected density of mammals of weighing 1 g. This density therefore represents the highest likely density of individuals, given that the smallest mammal is around 2 g ?. A total of 3937 individuals per simulation were created which were placed randomly at the start of the simulation. Individuals were assigned 11 signal detection widths  $\alpha$  between 0 and  $\pi$  ( $1/11\pi, 2/11\pi, 3/11\pi, 4/11\pi, 5/11\pi, 6/11\pi, 7/11\pi, 8/11\pi, 9/11\pi, 10/11\pi, \pi$ ).

Each simulation lasted for  $N$  steps (14400) of duration  $T$  (15 minutes) giving a total duration of 150 days. The individuals moved within each step with a distance  $d$ , with an average speed,  $v$ .  $d$ , was sampled from a normal distribution with mean distance,  $\mu_d = vT$ , and standard deviation  $\sigma_d = vT/10$ . An average speed,  $v = 40 \text{ km days}^{-1}$ , was chosen as this represents the largest day range of terrestrial animals (?), and represents the upper limit of realistic speeds. At the end step, individuals were allowed to either remain stationary for a time step (with a given probability,  $S$ ), change direction (with a maximum angle,  $A$ ) between 0 and  $\pi$ . This resulted in 7 different movement models where: (1) simple movement, where  $S$  and  $A = 0$ ; (2) stop-start movement, where (i)  $S = 0.25, A = 0$ , (ii)  $S = 0.5, A = 0$ , (iii)  $S = 0.75, A = 0$ ; (3) random walk movement, where (i)  $S = 0, A = \pi/3$ , (ii)  $S = 0, A = 2\pi/3$ , (iii)  $S = 0, A = \pi$ . Individuals were counted as they moved in and out of the detection zone of the sensor per simulation.

We calculated the estimated animal density from the gREM by summing the number of captures per simulation and inputting these values into the correct gREM submodel. gREM accuracy was determined by comparing the density in the simulation with the estimated density. High accuracy is indicated by the mean difference between the estimated and actual values not being significantly different from zero (Wilcoxon signed-rank test). gREM precision was determined by the standard deviation of estimated densities. We used this method to compare the accuracy and precision of all the gREM submodels. As these submodels are

247 derived for different combinations of  $\alpha$  and  $\theta$ , the accuracy and precision of the  
248 submodels was used to determine the impact of different values of  $\alpha$  and  $\theta$ .

249 The influence of the number of captures and animal movement models on accu-  
250 racy and precision was investigated using 4 different gREM submodels represen-  
251 tative of the range  $\alpha$  and  $\theta$  values (submodels NW1, SW1, NE1, and SE3, Figure 2).  
252 Using these four submodels, we calculated how long the simulation needed to  
253 run to generate a range of different capture numbers (from 10 to 100 captures in  
254 10 unit intervals), and estimated animal density. These estimated densities were  
255 compared to the real density to assess the impact on the accuracy and precision  
256 on the gREM of different simulation lengths. We also used these four submodels  
257 to compare the accuracy and precision of a simple movement model, to stop-start  
258 movement models and random walk movement models. The gREM assumes that  
259 individuals move continuously with straight-line movement (simple movement  
260 model) and we therefore assessed the impact of breaking the gREM assumptions.

## 261 4. RESULTS

262 4.1. **Analytical model.** The equation for  $\bar{p}$  has been newly derived for each sub-  
263 model in the gREM, except for the gas model and REM which have been calculated  
264 previously. However, many models, although derived separately, have the same  
265 expression for  $\bar{p}$ . Figure 4 shows the expression for  $\bar{p}$  in each case. The general  
266 equation for density, using the correct expression for  $\bar{p}$  is then substituted into  
267 eqn 3. Although more thorough checks are performed in Appendix S3, it can be  
268 seen that all adjacent expressions in Figure 4 are equal when expressions for the  
269 boundaries between them are substituted in.

## 270 4.2. Simulation model.

271 4.2.1. *gREM submodels.* All gREM submodels showed a high accuracy, i.e., the  
272 mean difference between the estimated and actual values was not significantly  
273 different from zero across all models, corrected for multiple tests (all gREM sub  
274 models Wilcoxon signed-rank test,  $p > 0.002$ )(Figure 5). However, the precision of  
275 the submodels do vary, where the gas model is the most precise and the SW7 sub

model the least precise, having the smallest and the largest interquartile range, respectively (Figure 5). The standard deviation of the error between the estimated and true densities is strongly related to both the sensor and signal widths (Figure 6), such that larger widths have lower standard deviations (greater precision). However, even smaller sensor and signal widths have a relatively high level of precision.

4.2.2. *Number of captures.* Within the four gREM submodels tested (NW1, SW1, SE3, NE1), the accuracy was not affected by the number of captures, where the mean difference between the estimated and actual values was not significantly different from zero across all capture rates, corrected for multiple tests (all gREM submodels Wilcoxon signed-rank test,  $p > 0.008$ ) (Figure 7). However, the precision was dependent on the number of captures across all four of the gREM submodels, where precision increases as number of captures increases (Figure 7). For all gREM submodels, the coefficient of variation falls to 10% at 100 captures.

4.2.3. *Movement models.* Within the four gREM submodels tested (NW1, SW1, SE3, NE1), neither the accuracy or precision was affected by the amount of time spent stationary. The mean difference between the estimated and actual values was not significantly different from zero for each category of stationary time (0, 0.25, 0.5 and 0.75), corrected for multiple tests (all gREM submodels Wilcoxon signed-rank test,  $p > 0.12$ ) (Figure 8a). Altering the maximum change in direction in each step (0,  $\pi/3$ ,  $2\pi/3$ , and  $\pi$ ) did not affect the accuracy or precision of the four gREM submodels tested (all gREM submodels Wilcoxon signed-rank test,  $p > 0.05$ ) (Figure 8b).

## 5. DISCUSSION

We have developed the gREM such that it can be used to estimate density from acoustic sensors and camera traps. This has entailed a generalisation of the model and the REM in (?) to be applicable to any combination of sensor width and signal directionality. We have used simulations to show, as a proof of principle, that these models are accurate and precise. The precision of the gREM was

found to be dependent on the width of the sensor and the call, and the number of captures.

**5.1. Analytical model.** The gREM was derived for different combinations of  $\alpha$  and  $\theta$  resulting in 25 different submodels, the expression for  $\bar{p}$  are equal for many of these submodels resulting in 8 different equations including the previously derived gas model and REM. These submodels were tested for consistency with adjacent expressions being equal at their boundaries. These new submodels will allow researchers to evaluate the absolute density of animals that have previously been difficult to study with noninvasive methods such as remove sensors. The gREM allows the data from acoustic detectors to be used where an animal has a directional calls, this could be used for a range of animals including bats, songbirds, Cetaceans and forest primates.

There are a number of positive extensions to the gREM which could be developed in the future. The original gas model was formulated for the case where both subjects, either animal and detector, or animal and animal, are moving (?). Indeed any of the models with animals that are equally detectable in all directions ( $\alpha = 2\pi$ ) can be trivially expanded for moving by substituting the sum of the average animal velocity and the sensor velocity for  $v$  as used here. However, when the animal has a directional call, the extension becomes less simple. The approach would be to calculate again the mean profile width. However, for each angle of approach, one would have to average the profile width for an animal facing in any direction (i.e. not necessarily moving towards the sensor) weighted by the relative velocity of that direction. There are a number of situations where a moving detector and animal could occur and as such may be advantage to have a method of estimating densities from the data collected, e.g. an acoustic detector based off a boat when studying Cetacea or sea birds (?). Another interesting, and so far unstudied problem, is edge effects caused by trigger delays (the delay between sensing an animal and attempting to record the encounter) and time expansion acoustic detectors which repeatedly turn on an off during sampling. Both of these have potential biases as animals can move through the detection zone without being detected.

335 The models herein are formulated assuming constant surveillance and so the er-  
336 ror quickly becomes negligible. For example, if it takes longer for the recording  
337 device to be switched on than the length of some animal calls there could be a  
338 systematic underestimation of density.

339 **5.2. Accuracy and Precision.** We tested each of the gREM submodels for accuracy  
340 and precision through a simulation. All the submodels produced estimated den-  
341 sities that were not significantly different from the true density of the simulation.  
342 Therefore based on these simulations we believe that the gREM has the poten-  
343 tial to produce accurate estimates for many different species, using either camera  
344 traps or acoustic detectors. However the precision of the gREM differed between  
345 submodels. For example, when the sensor and signal width were smaller then the  
346 precision of the model was reduced, so when choosing a sensor for use in a gREM  
347 study the detection width should be maximised, and if the study species has a  
348 narrow signal directionality other aspects of the study protocol should be used to  
349 compensate.

350 The precision of the gREM is greatly affected by the number of captures that are  
351 collected, the coefficient of variation falls dramatically between 10 and 60 captures  
352 and then after this continues to slowly reduce. At 100 captures the submodels  
353 reach 10% coefficient of variation, and therefore we believe at this point the models  
354 are precise. The length of surveys in the field will need to be adjusted so that  
355 enough data is collected to reach this level of precision, populations of fast moving  
356 animals or populations with large densities will require less survey effort than  
357 those with slow moving or low densities.

358 The gREM was both accurate and precise for all the movement models we  
359 tested against, stop-start movement and correlated random walks. However these  
360 movement models are still simple representations of true animal movement which  
361 often consist of multiple be dependent on multiple factors such as behavioural  
362 state and and existence of home ranges (?). The accuracy of the gREM may be  
363 affected by the interaction between the movement model and the size of the detec-  
364 tion radius. In figure 8b we studied a relatively long step length compared to the  
365 size of the detection radius, and therefore the chance of catching the same animal

multiple times within a short space of time was reduced. However if the ratio of step length to detection radius was smaller then this may decrease the precision of the model, however this should not decrease its accuracy.

Although we have used simulations to validate the gREM submodels, much more robust testing is needed. Although difficult, proper field test validation would be required before the models could be fully trusted. The REM (?) has already been field tested, and both ? and ? both found that the REM was an effective manner of estimating animal densities (??). In some taxa gold standard methods of estimating animal density exist, such as capture mark recapture. Where these gold standard exist, and have been proved to work, a simultaneous gREM study could be completed to test the accuracy under field conditions. An easier way to continue to evaluate the models is to run more extensive simulations which break the assumptions of the analytical models. The main element that cannot be analytically treated is the complex movement of real animals. Therefore testing these methods against true animal traces, or more complex movement models would be required.

Within the simulation we have assumed an equal density across the entire world, however in a field environment the situation would be much more complex, with additional variation coming from local changes in density between camera sites. In the simulation we ran the speed of the animal as  $40 \text{ km days}^{-1}$ , the largest day range of terrestrial animals (?), other speed values should not alter the accuracy or the precision of the gREM. We also assume perfect knowledge of the average speed of an animal and size of the detection zone, and instant triggering of the camera. All of which may lead to possible bias or a decrease in precision.

**5.3. Implications for conservation.** The gREM is therefore available for the estimation of density of a number of taxa of importance to conservation, zoonotic diseases and ecosystem services. The models provided are suitable for certain groups for which there are currently no, or few, effective methods for density estimation. Any species that would be consistently recorded at least once when within range of a detector would be a suitable subject for the gREM, such as bats (?), songbirds

396 (?), Cetaceans (?) or forest primates (?). Within increasing technological capabili-  
397 ties, this list of species is likely to increase dramatically.

398 Importantly the methods are noninvasive and do not require human marking or  
399 naturally identifying marks (as required for mark-recapture models). This makes  
400 them suitable for large, continuous monitoring projects with limited human re-  
401 sources. It also makes them suitable for species that are under pressure, species  
402 that cannot naturally be individually recognised or species that are difficult or  
403 dangerous to catch.

404 6. ACKNOWLEDGMENTS

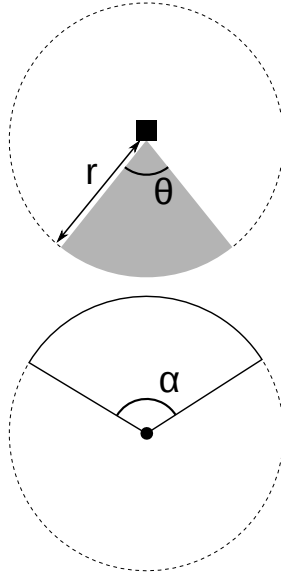


FIGURE 1. Representation of sensor detection width and animal signal width. The filled square and circle represent a sensor and an animal, respectively;  $\theta$ , sensor detection width (radians);  $r$ , sensor detection distance; dark grey shaded area, sensor detection zone;  $\alpha$ , animal signal width (radians). Dashed lines around the filled square and circle represents the maximum extent of  $\theta$  and  $\alpha$ , respectively.



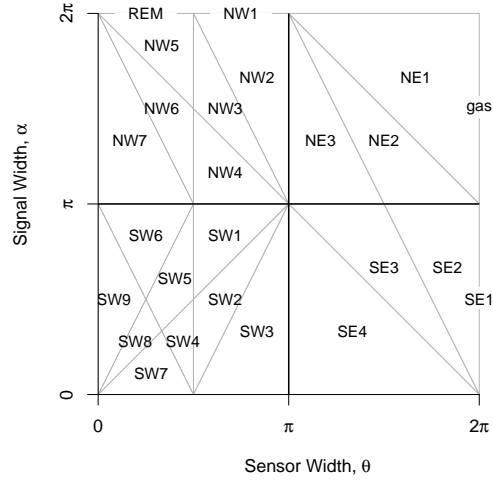


FIGURE 2. Locations where derivation of the average profile  $\bar{p}$  is the same for different combinations of sensor detection width and animal signal width. Symbols within each polygon refer to each gREM submodel named after their compass point, except for Gas and REM which highlight the position of these previously derived models within the gREM. Symbols on the edge of the plot are for submodels with  $\alpha, \theta = 2\pi$

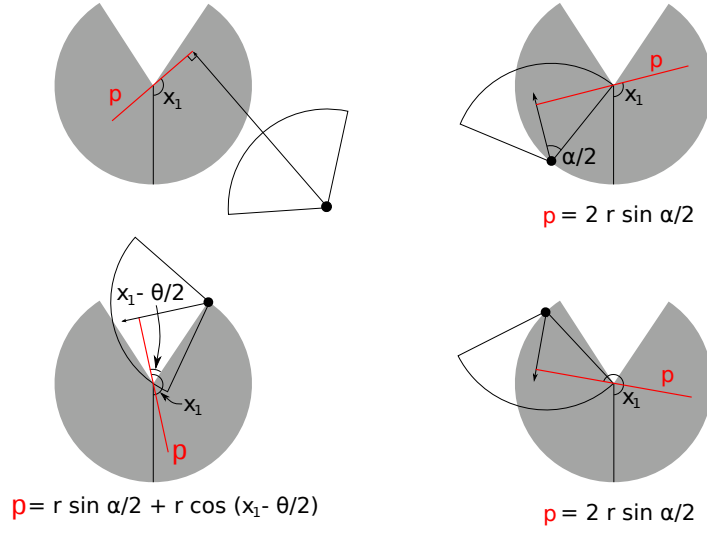


FIGURE 3. An overview of the derivation of SE2. The filled circles represent animals, with the animal signal shown as a unfilled sector and the direction of movement shown as an arrow. The detection zone of the sensors are shown as filled grey sectors with a detection distance of  $r$ . The SYMBOL shows the direction the sensor is facing;  $\theta$ , sensor detection width;  $\alpha$ , animal signal width. The profile  $p$  (the line an animal must pass through in order to be captured) is shown in red and  $x_1$  is the focal angle, where (a) shows the location of  $x_1$ . The derivation of  $p$  changes as the animal approaches the sensor from different directions where (b) is the derivation of  $p$  when  $x_1$  is in the interval  $[\frac{\pi}{2}, \frac{\pi}{2} + \frac{\theta}{2} - \frac{\alpha}{2}]$ , (c)  $p$  when  $x_1$  is in the interval  $[\frac{\pi}{2} + \frac{\theta}{2} - \frac{\alpha}{2}, \frac{5\pi}{2} - \frac{\theta}{2} - \frac{\alpha}{2}]$  and (d)  $p$  when  $x_1$  is in the interval  $[\frac{5\pi}{2} - \frac{\theta}{2} - \frac{\alpha}{2}, \frac{3\pi}{2}]$ . The resultant equation for  $p$  is shown beneath each figure.

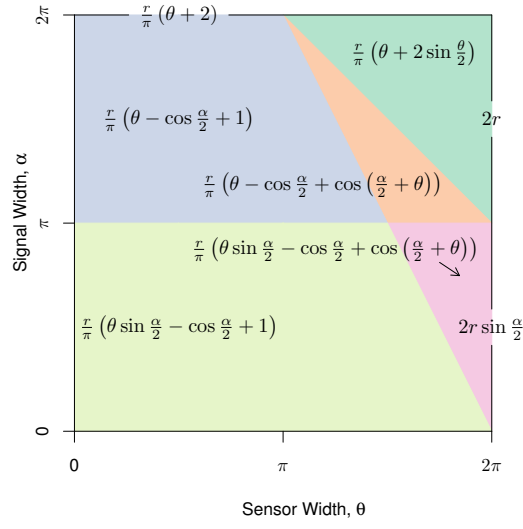


FIGURE 4. Expressions for the average profile width,  $\bar{p}$ , given sensor and signal widths. Despite independent derivation within each block, many models result in the same expression. These are collected together and presented as one block of colour. Expressions on the edge of the plot are for submodels with  $\alpha, \theta = 2\pi$ .

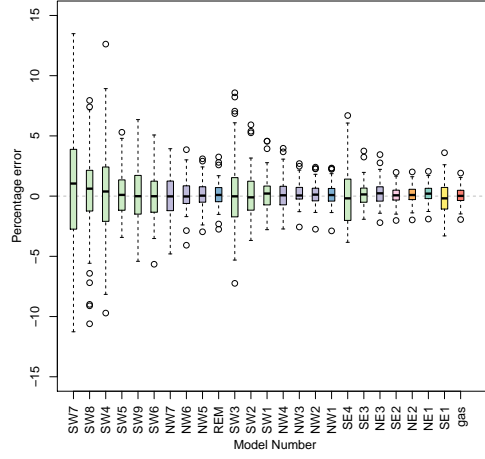


FIGURE 5. Simulation model results of the accuracy and precision for gREM submodels. The percentage error between estimated and true density for each gREM submodel is shown within each box plot, where the black line represents the median percentage error across all simulations, boxes represent the the middle 50% of the data. Box colours correspond to the expressions for average profile width  $\bar{p}$  given in Figure 4.

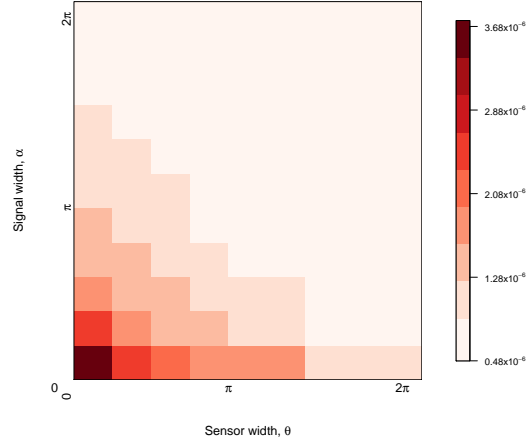


FIGURE 6. Simulation model results of the gREM precision given a range of sensor and signal widths, shown by the standard deviation of the error between the estimated and true densities. Standard deviations are shown from deep red to pink, representing high to low values between  $0.483 \times 10^{-6}$  to  $3.74 \times 10^{-6}$ .

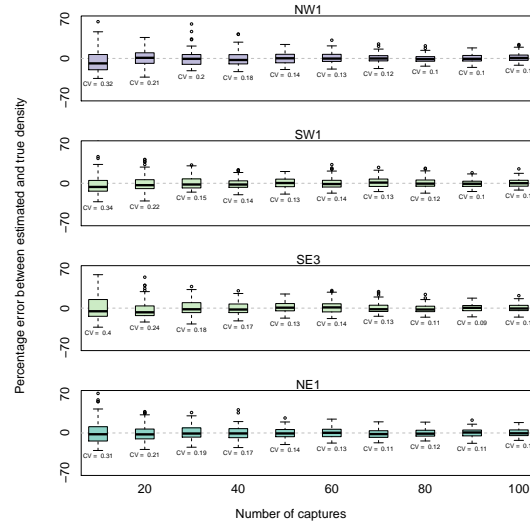


FIGURE 7. Simulation model results of the accuracy and precision of four gREM submodels (NW1, SW1, SE3 and NE1) given different numbers of captures. The percentage error between estimated and true density within each gREM sub model for capture rate is shown within each box plot. Sensor and signal widths vary between submodels. The colour of each box plot corresponds to the expressions for average profile width  $\bar{p}$  given in Figure 4.

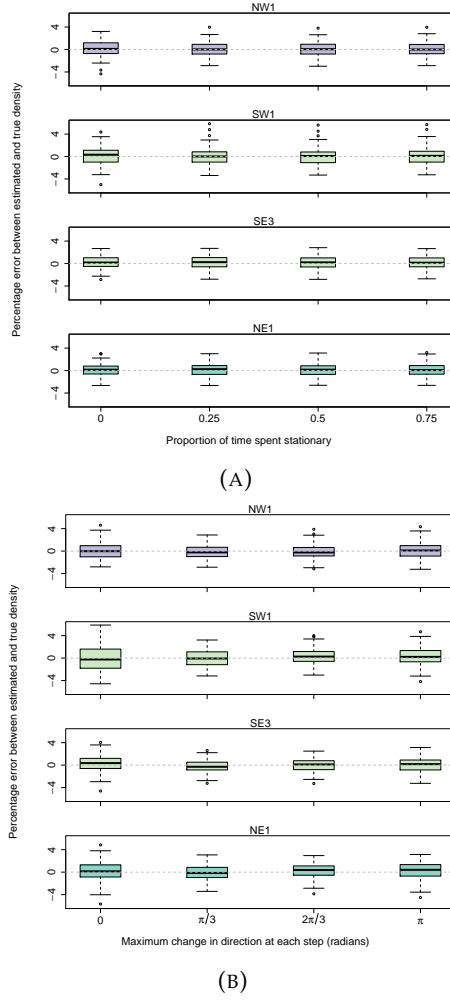


FIGURE 8. Simulation model results of the accuracy and precision of four gREM submodels (NW1, SW1, SE3 and NE1) given different movement models where (A) amount of time spent stationary (stop-start movement) and (B) maximum change in direction at each step (correlated random walk model). The percentage error between estimated and true density within each gREM sub model for the different movement models is shown within each box plot. The simple model is represented where time and maximum change in direction equals 0. The colour of each box plot corresponds to the expressions for average profile width  $\bar{p}$  given in Figure 4.